Electronic Supplementary Material (ESI) for Inorganic Chemistry Frontiers.

Supporting Information

Light Actuated Single-Chain Magnet with Magnetic Coercivity

Qiang Liu,[a] Nian-Tao Yao,[a] Hui-Ying Sun,[a] Ji-Xiang Hu,[b] Yin-Shan Meng*[a] and Tao Liu[a]

[a]*State Key Laboratory of Fine Chemicals, Dalian University of Technology, Dalian, 116024, China*
[b]*College of Chemistry and Chemical Engineering, Qingdao University, Qingdao, 266071, China*

*Corresponding authors. Email: mengys@dlut.edu.cn

CONTENTS

Table S1. Crystal data and structure refinements for compound **1**.

T (K)	273	110
Formula	$C_{36}H_{29}B_2CoFe_2N_{28}O_4$	$C_{36}H_{29}B_2CoFe_2N_{28}O_4$
CCDC	2160263	2160264
Fw	1110.12	1110.12
Crystal system	Triclinic	Triclinic
Space group	$P\bar{1}$	$P\bar{1}$
a (Å)	12.1414(15)	11.714(3)
b (Å)	14.1379(17)	13.736(3)
c (Å)	14.5464(17)	14.694(3)
α (º)	84.704(4)	87.693(8)
β (º)	81.780(4)	80.355(7)
γ (º)	87.586(4)	89.333(7)
V (Å^3)	2459.7(5)	2329.1(9)
Z	1	1
ρ_{calc} (g/cm^3)	1.499	1.583
F (000)	1124.0	1124.0
Reflections collected	38448	41701
Unique reflections (R_{int})	0.0962	0.0801
Goodness-of-fit on F^2	1.133	1.213
R_1, [$I \geq 2\sigma(I)$]	0.1404	0.1220
wR_2, [$I \geq 2\sigma(I)$]	0.2996	0.2582

$R_1 = \Sigma||F_o|-|F_c|| / \Sigma|F_o|$; $wR_2 = \{\Sigma[w(F_o^2-F_c^2)^2] / \Sigma[w(F_o^2)^2]\}^{1/2}$.

Table S2. Crystal data and structure refinements for compound **2**.

T (K)	230	150
Formula	$C_{30}H_{26}B_2CoFe_2N_{24}O_4$	$C_{30}H_{26}B_2CoFe_2N_{24}O_4$
CCDC	2160261	2160262
Fw	979.00	979.00
Crystal system	Monoclinic	Monoclinic
Space group	$P2_1/n$	$P2_1/n$
a (Å)	12.0759(11)	11.7234(6)
b (Å)	14.0951(13)	13.8376(8)
c (Å)	28.122(3)	27.9557(17)
α (º)	90	90
β (º)	90.258(3)	91.839(2)
γ (º)	90	90
V (Å^3)	4786.6(8)	4532.7(4)
Z	4	4
ρ_{calc} (g/cm^3)	1.358	1.515
F (000)	1980.0	2088.0
Reflections collected	38837	37680
Unique reflections (R_{int})	0.0735	0.0515
Goodness-of-fit on F^2	1.030	1.028
R_1, [$I \geq 2\sigma(I)$]	0.0835	0.0623
wR_2, [$I \geq 2\sigma(I)$]	0.2350	0.1674

$R_1 = \Sigma||F_o|-|F_c|| \,/\, \Sigma|F_o|$; $wR_2 = \{\Sigma[w(F_o^2-F_c^2)^2] \,/\, \Sigma[w(F_o^2)^2]\}^{1/2}$.

Table S3. Selected distances (Å) and angles (°) for **1** at different temperature.

Compound **1**	273 K	110 K		273 K	110 K
Bond length (Å)			Bond angle (°)		
Co1–N1[1]	2.153(9)	1.960(7)	N2–Co1–N1	89.4(4)	90.0(3)
Co1–N1	2.153(9)	1.960(7)	N2–Co1–N1[1]	90.6(4)	90.0(3)
Co1–N2[1]	2.096(10)	1.880(7)	N2[1]–Co1–N1[1]	89.4(4)	90.0(3)
Co1–N2	2.096(10)	1.880(7)	N2[1]–Co1–N1	90.6(4)	90.0(3)
Co1–N3[1]	2.095(11)	1.885(8)	N3[1]–Co1–N2	91.4(4)	90.1(3)
Co1–N3	2.095(11)	1.885(8)	N3–Co1–N2[1]	91.4(4)	90.1(3)
Co2–N4	2.141(9)	1.942(7)	N3–Co1–N2	88.6(4)	89.9(3)
Co2–N4[3]	2.141(9)	1.942(7)	N3[1]–Co1–N2[1]	88.6(4)	89.9(3)
Co2–N5	2.138(10)	1.900(8)	N3[1]–Co1–N1[1]	91.4(4)	91.3(3)
Co2–N5[3]	2.138(10)	1.900(8)	N3[1]–Co1–N1	88.6(4)	88.7(3)
Co2–N7	2.109(10)	1.881(7)	N3–Co1–N1	91.4(4)	91.3(3)
Co2–N7[4]	2.109(10)	1.881(7)	N3–Co1–N1[1]	88.6(4)	88.7(3)
Fe1–N22	1.951(8)	1.963(7)	N5[3]–Co2–N4[3]	90.3(4)	90.3(3)
Fe1–N24	1.956(10)	1.996(8)	N5–Co2–N4	90.3(4)	90.3(3)
Fe1–N26	1.981(11)	1.987(9)	N5–Co2–N4[3]	89.7(4)	89.7(3)
Fe1–C2	1.921(13)	1.886(9)	N5[3]–Co2–N4	89.7(4)	89.7(3)
Fe1–C5	1.908(12)	1.884(10)	N7[1]–Co2–N5[3]	86.9(4)	89.9(3)
Fe1–C8	1.876(15)	1.866(9)	N7[4]–Co2–N5	86.9(4)	89.9(3)
Fe2–N17	1.953(9)	1.976(7)	N7[4]–Co2–N5[3]	93.1(4)	90.1(3)
Fe2–N13	1.941(9)	1.951(7)	N7[1]–Co2–N5	93.1(4)	90.1(3)
Fe2–N15	1.944(9)	1.972(7)	N7[1]–Co2–N4	90.9(4)	91.8(3)
Fe2–C3	1.930(13)	1.884(9)	N7[1]–Co2–N4[3]	89.1(4)	88.2(3)
Fe2–C6	1.908(15)	1.896(10)	N7[4]–Co2–N4	89.1(4)	88.2(3)
Fe2–C7	1.907(12)	1.906(8)	N7[4]–Co2–N4[3]	90.9(4)	91.8(3)

Symmetry transformations used to generate equivalent atoms: [1]1-X, 1-Y, 1-Z; [2]+X, -1+Y, +Z; [3]1-X, 2-Y, 1-Z; [4]+X, 1+Y, +Z; [5]2-X, 1-Y, 1-Z; [6]-X, 2-Y, 1-Z.

Table S4. Selected distances (Å) and angles (°) for **2** at different temperature.

Compound **2**	230 K	150 K		230 K	150 K
Bond length (Å)			Bond angle (°)		
Co1–N1	2.117(5)	1.928(3)	N1–Co1–N2[1]	178.8(2)	179.14(16)
Co1–N2[1]	2.120(5)	1.935(3)	N3–Co1–N1	90.0(2)	89.64(15)
Co1–N3	2.072(6)	1.888(4)	N3–Co1–N2[1]	89.0(2)	89.50(15)
Co1–N4	2.107(6)	1.890(4)	N3–Co1–N4	88.0(2)	90.12(16)
Co1–N6[2]	2.082(6)	1.891(4)	N3–Co1–N6[2]	178.8(2)	179.42(15)
Co1–N8[3]	2.108(6)	1.892(4)	N3–Co1–N8[3]	92.5(2)	90.16(16)
Fe1–N20	1.970(6)	1.993(4)	N4–Co1–N1	92.5(2)	91.26(15)
Fe1–N22	1.997(6)	2.010(4)	N4–Co1–N2[1]	88.2(2)	88.83(15)
Fe1–N24	1.986(6)	1.996(4)	N4–Co1–N8[3]	179.5(2)	89.88(16)
Fe1–C4	1.910(7)	1.868(4)	N6[2]–Co1–N1	91.0(2)	179.64(17)
Fe1–C5	1.909(8)	1.908(5)	N6[2]–Co1–N2[1]	90.0(2)	90.93(15)
Fe1–C8	1.912(7)	1.878(4)	N6[2]–Co1–N4	91.3(2)	89.93(15)
Fe2–N13	1.965(6)	1.959(4)	N6[2]–Co1–N8[3]	88.3(2)	89.85(16)
Fe2–N16	1.967(6)	1.976(4)	N8[3]–Co1–N1	87.2(2)	88.50(15)
Fe2–N17	1.969(6)	1.974(4)	N8[3]–Co1–N2[1]	92.1(2)	91.42(15)
Fe2–C3	1.896(7)	1.907(4)	---	---	---
Fe2–C6	1.899(7)	1.913(4)	---	---	---
Fe2–C7	1.915(7)	1.916(5)	---	---	---

Symmetry transformations used to generate equivalent atoms: [1]-1+X, +Y, +Z; [2]1/2-X, -1/2+Y, 3/2-Z; [3]1/2-X, 1/2+Y, 3/2-Z; [4]1+X, +Y, +Z.

Table S5. Temperature-dependent ^{57}Fe Mössbauer parameters for **1** and **2**.

	T (K)	δ (mm s^{-1})	ΔE_Q (mm s^{-1})	Relative area (%)	Approximation ratio	Fe type
	290 K	−0.10	0.90	100	---	Fe^{III}_{LS}
1	80 K	0.08	0.45	49.18	1	Fe^{II}_{LS}
		−0.06	1.42	50.82	1	Fe^{III}_{LS}
	240 K	−0.02	0.98	100	---	Fe^{III}_{LS}
2	75 K	0.15	0.52	48.76	1	Fe^{II}_{LS}
		0.02	1.23	51.24	1	Fe^{III}_{LS}

Table S6. Selected distances (Å) in compounds **1** and **2**.

	T (K)	$Co^{II}\cdots Co^{II}$ intrachain	$Co^{II}\cdots Co^{II}$ interchain	hydrogen bonding	π···π interaction
1	273	7.069(9)	12.141(2)	2.86(2), 2.96(3)	3.605(9)
	110	6.868(2)	11.714(3)	2.816(16), 2.93(2)	3.601(5)
2	230	7.054(5)	12.076(2)	2.760(15), 2.894(1)	3.673(4), 3.916(4)
	150	6.924(4)	11.723(6)	2.745(9), 2.875(8)	3.639(3), 3.886(3)

Table S7. Comparison of energy barrier data in photo-induced [FeCo]-based nanomagnets.

Complex	H_{dc} (Oe)	$\Delta E/k_B$ (K)	Coercive field (Oe)	Ref.
$\{[Fe(^{pz}Tp)(CN)_3]_2Co(4\text{-styrylpyridine})_2\}\cdot 2H_2O\cdot 2CH_3OH$	0	27	---	S1
$\{[Fe(bpy)(CN)_4]_2Co(4,4'\text{-bipyridine})\}\cdot 4H_2O$	0	29	---	S2
$[Co((R)\text{-pabn})][Fe(Tp)(CN)_3](BF_4)\cdot H_2O$	0	66	---	S3
$[Co_2Fe_4(bimpy)_2(CN)_6(\mu\text{-}CN)_6(^{pz}Tp)_4]\cdot 2(1\text{-PrOH})\cdot 4H_2O$	500	26	---	S4
$\{[Fe(bpy)(CN)_4]_2Co(phpy)_2\}\cdot 2H_2O$	0	40	---	S5
$\{[Fe(Tp)(CN)_3]_2(Co(dpa)_2)\}\cdot 2H_2O$	2000	---	---	S6
$\{[Fe(Tp)(CN)_3]_2Co(BIT)\}\cdot 2CH_3OH$	0	43	50	S7
$\{[(^{Pz}Tp)Fe(CN)_3]_2Co(\mathbf{L})_2\}\cdot 4H_2O$	0	81	400	this work

Table S8. Selected Angles (°) in compounds **1** and **2**.

	1		**2**
	273 K		230 K
Co1–N3–C3	155.9(2)	Co1–N4–C4	155.5(5)
Co1–N2–C2	176.5(9)	Co1–N3–C3	175.2(5)
Co2–N7–C7	156.2(9)	Co1–N8–C8	161.5(5)
Co2–N5–C5	175.3(9)	Co1–N4–C4	171.4(5)

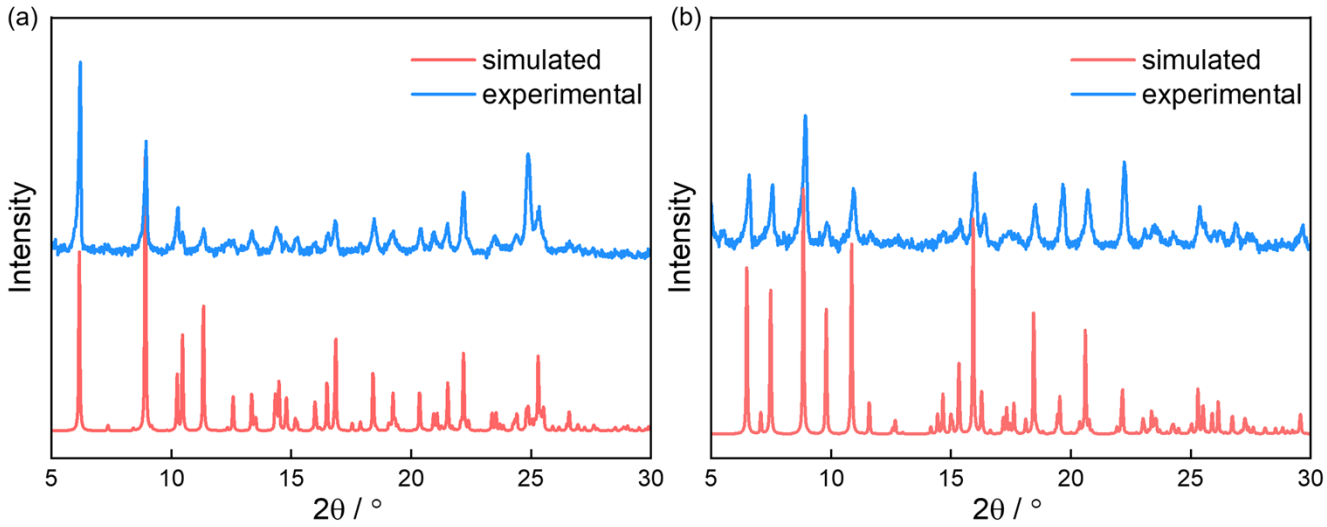

Fig. S1. X-ray powder diffraction data for compounds **1** (a) and **2** (b) at 300 K.

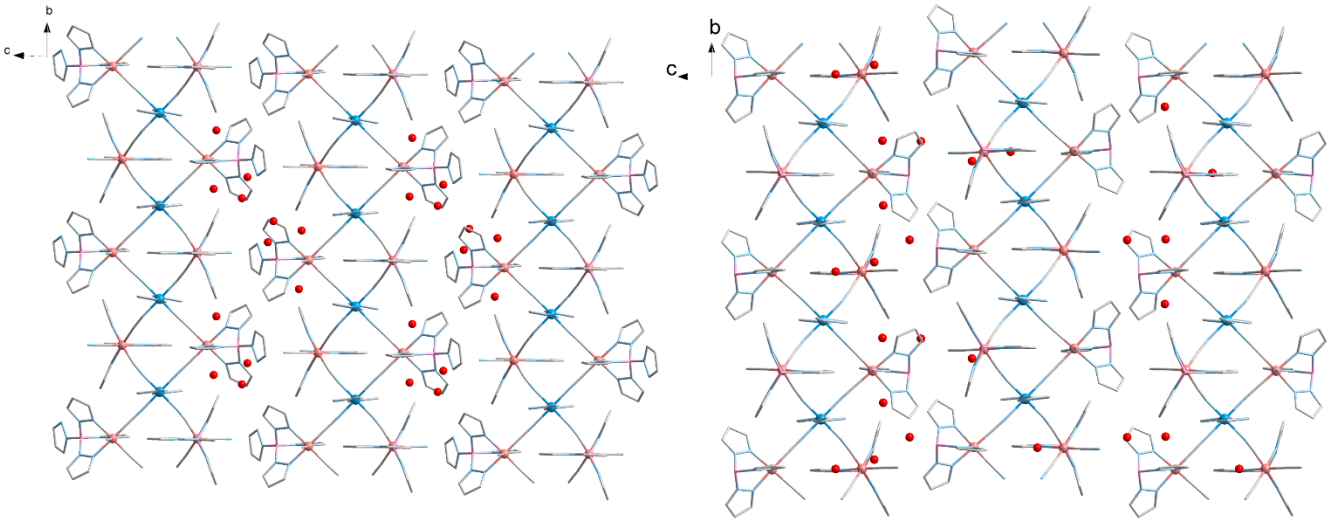

Fig. S2. Packing diagrams of **1** (left) and **2** (right) along *a* axis. Color code: Co^{II}, blue; Fe^{III}, red; B, violet; C, grey; N, pale blue; O, red. Hydrogen atoms were omitted for clarity.

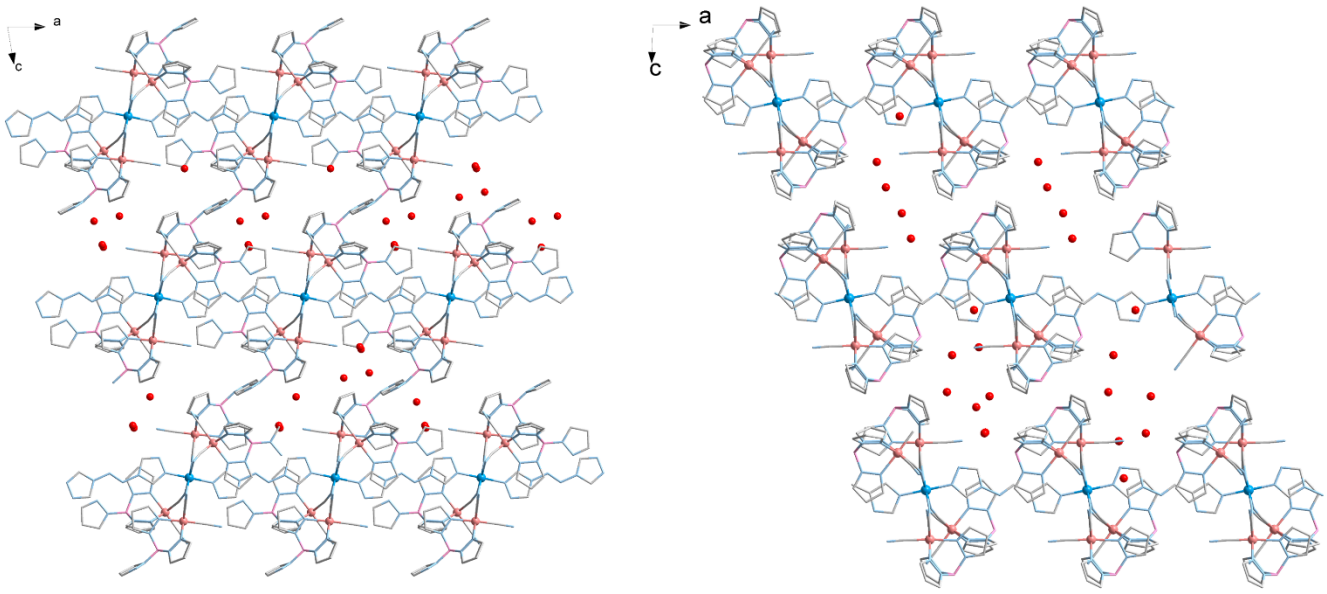

Fig. S3. Packing diagrams of **1** (left) and **2** (right) along *b* axis. Color code: Co^{II}, blue; Fe^{III}, red; B, violet; C, grey; N, pale blue; O, red. Hydrogen atoms were omitted for clarity.

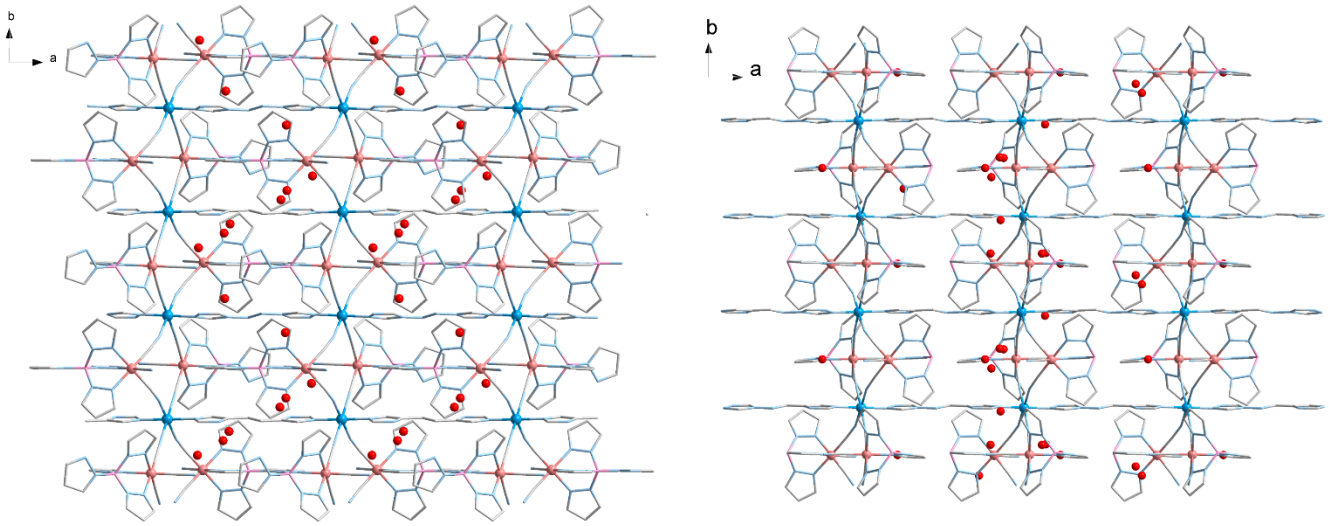

Fig. S4. Packing diagrams of **1** (left) and **2** (right) along *c* axis. Color code: Co^{II}, blue; Fe^{III}, red; B, violet; C, grey; N, pale blue; O, red. Hydrogen atoms were omitted for clarity.

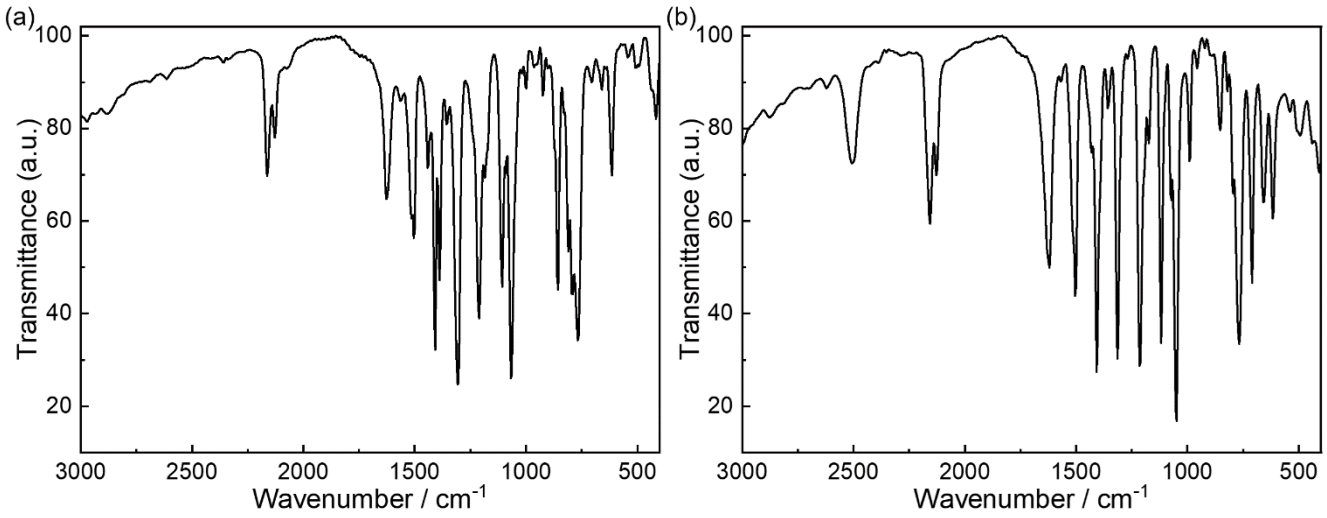

Fig. S5. IR spectra of **1** (a) and **2** (b) at 300 K.

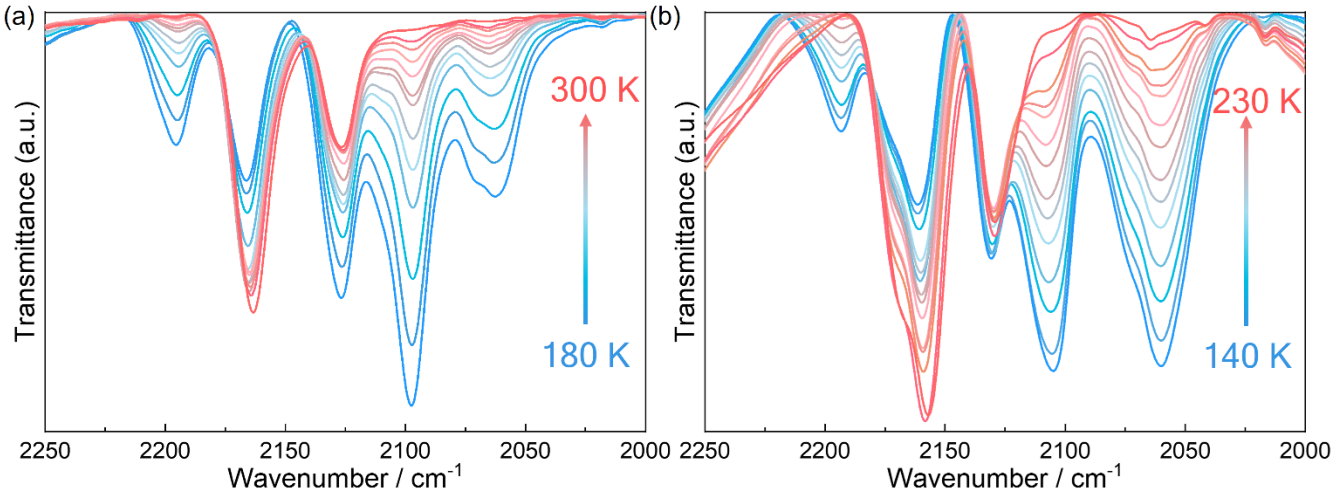

Fig. S6. Temperature-dependent infrared spectra in heating mode (from blue to red) for compounds **1** (a) and **2** (b).

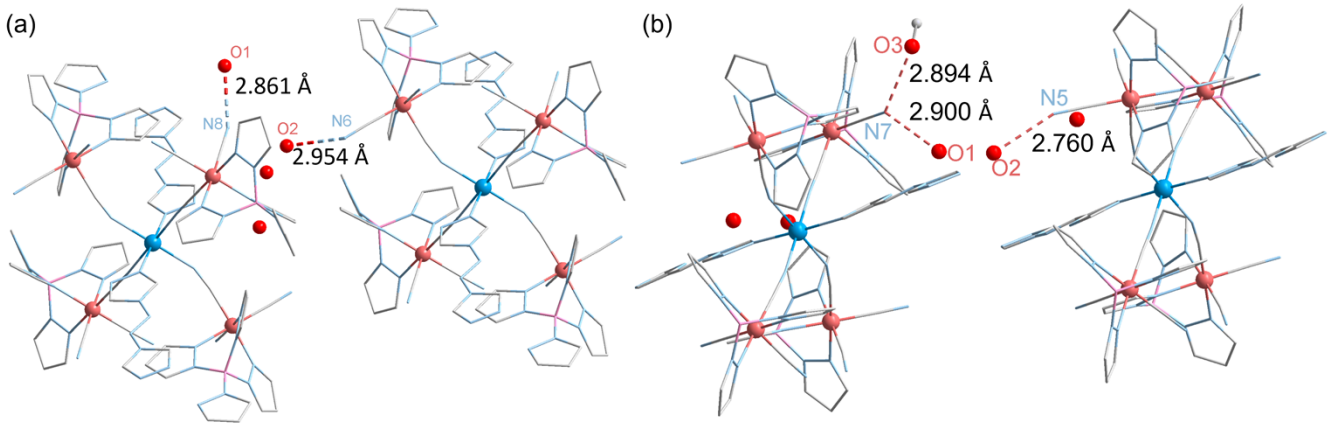

Fig. S7. Hydrogen bonds formed between lattice water molecules and terminal cyanide nitrogen atoms for **1** (a) at 273 K and **2** (b) at 230 K, respectively. Hydrogen atoms have been omitted for clarity.

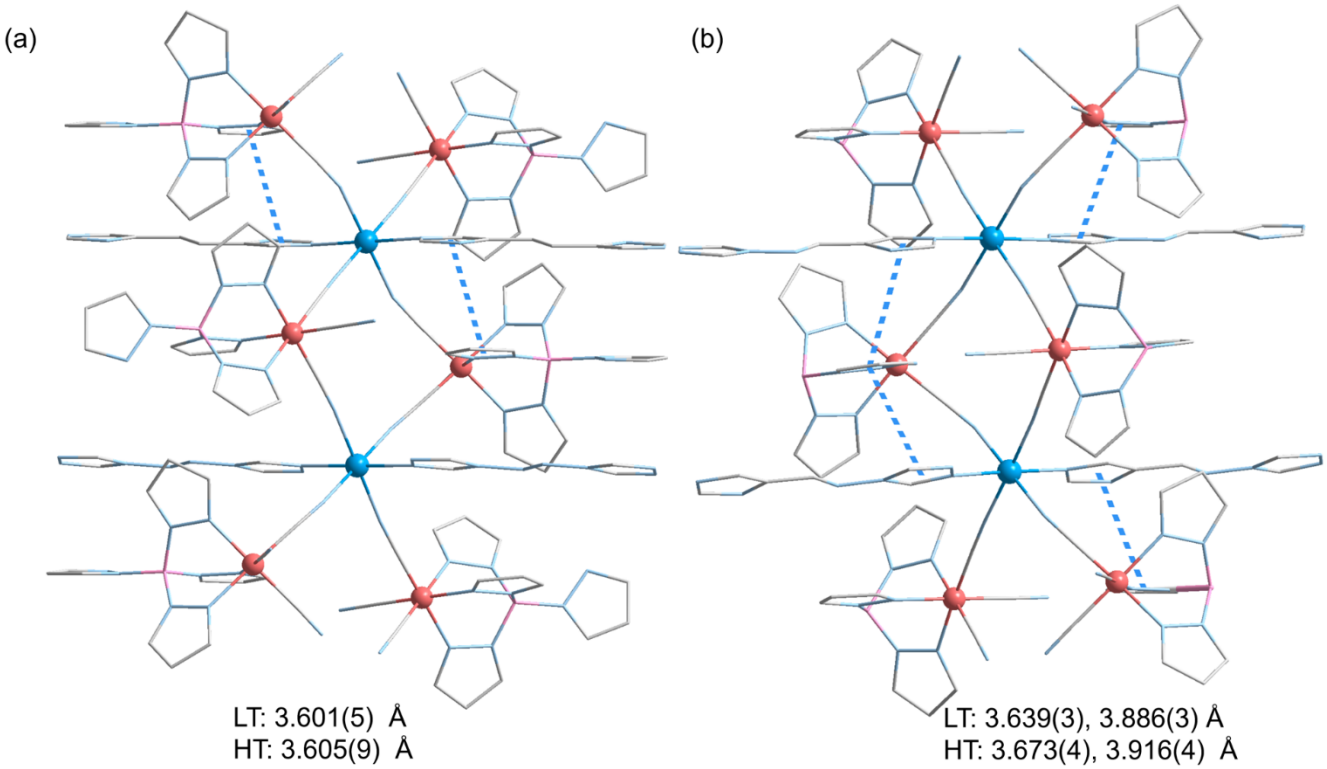

Fig. S8. π···π distances formed between ligand **L** and cyanometallate building blocks for **1** (a) and **2** (b) at LT and HT phases, respectively. Hydrogen atoms have been omitted for clarity.

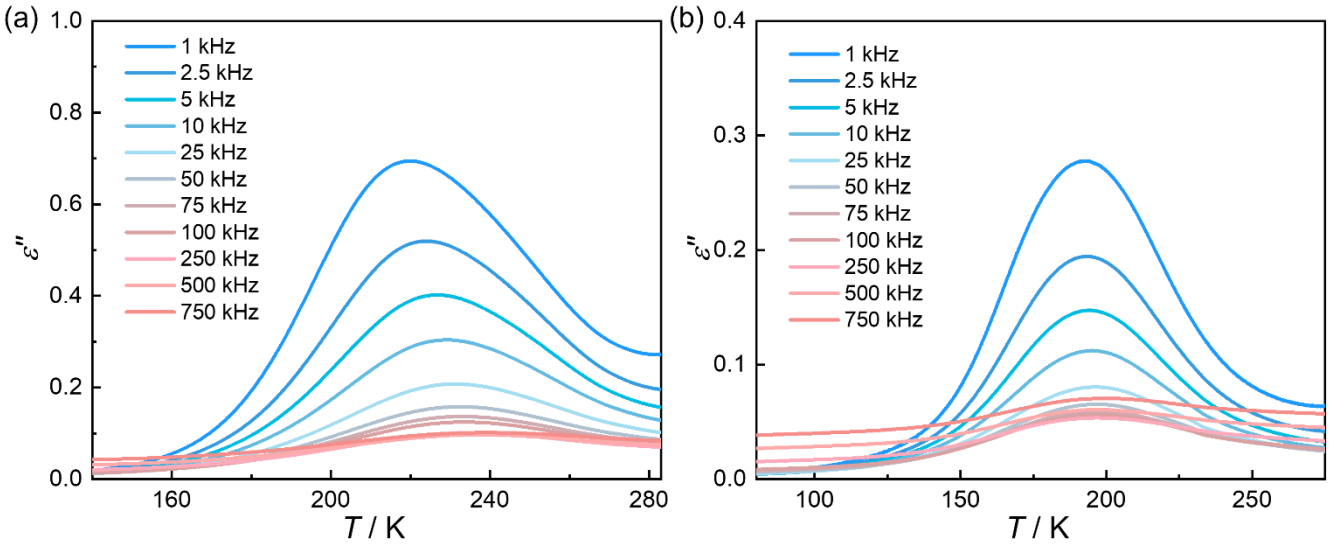

Fig. S9. Temperature-dependence dielectric loss (ε") signals of compounds **1** (a) and **2** (b) with different frequencies.

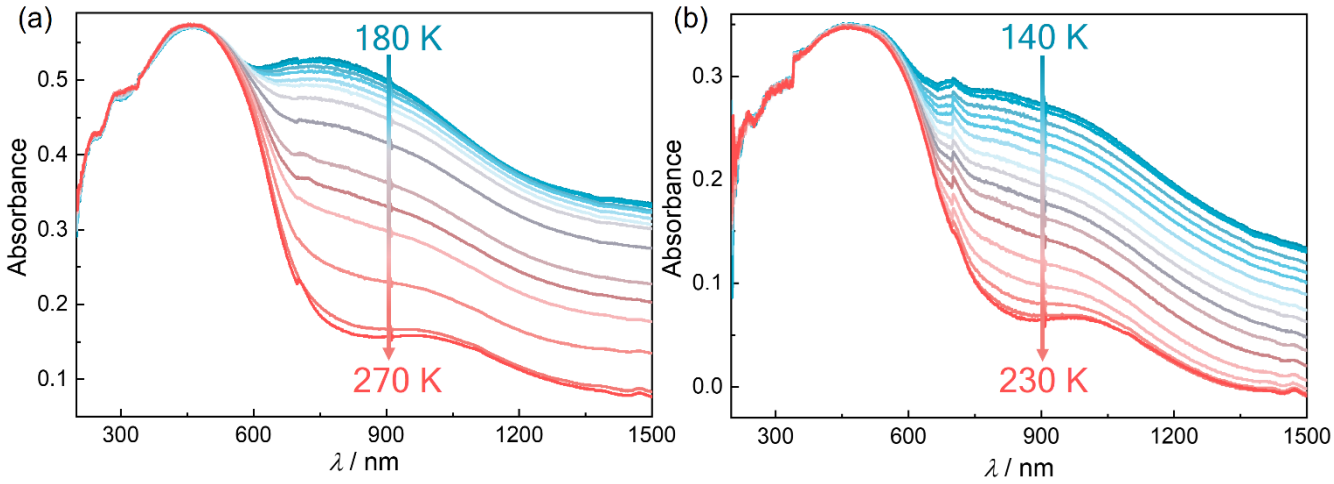

Fig. S10. Variable temperature solid state UV-Vis-NIR spectra in heating mode (from blue to red) for compounds **1** (a) and **2** (b).

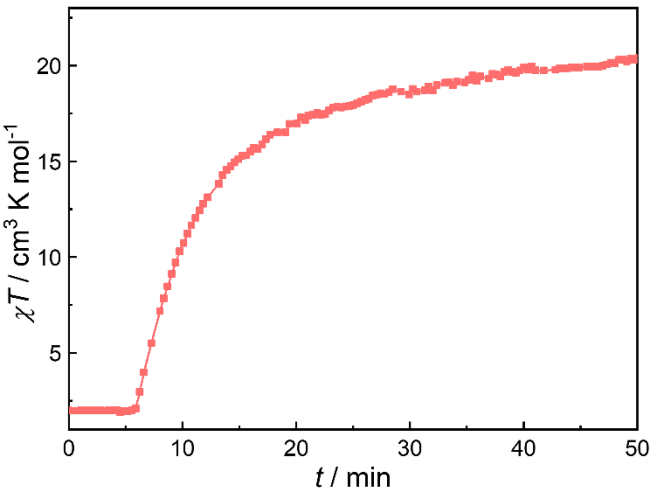

Fig. S11. χT vs time plots of **1** under successive 946-nm light irradiation at 10 K.

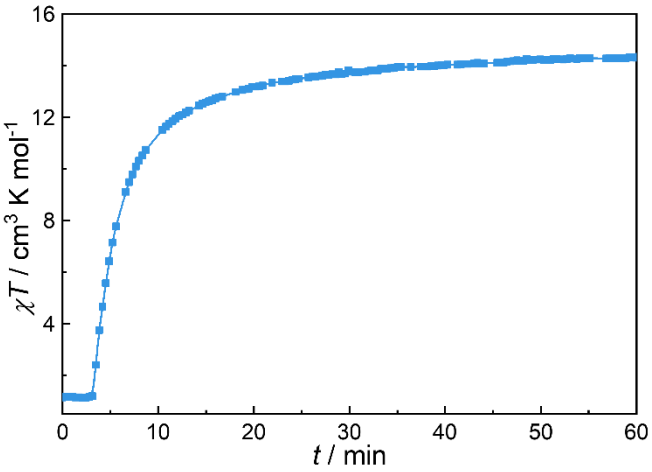

Fig. S12. χT vs time plots of **2** under successive 946-nm light irradiation at 10 K.

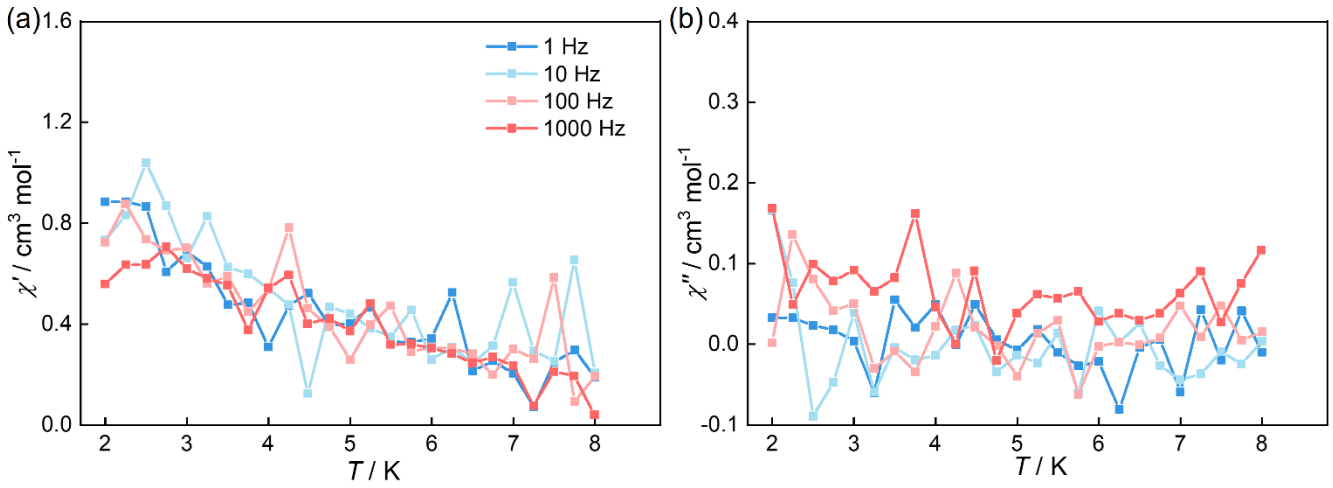

Fig. S13. Temperature dependence of in-phase (χ') and out-of-phase (χ'') signals for **1** before irradiation under zero DC field and 3.5 Oe AC field.

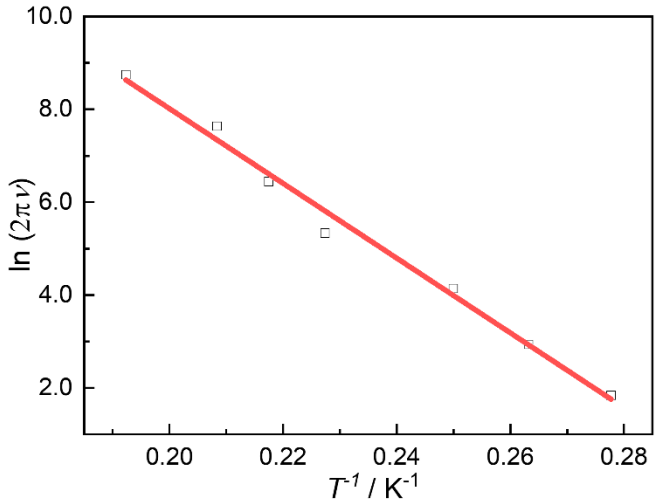

Fig. S14. ln ($2\pi f$) vs. T^{-1} plots for **1** after 946-nm light irradiation. The relaxation times $\tau = (2\pi f)^{-1}$ were determined from AC measurement. The solid line represented the least-squares fitting by applying the Arrhenius Law ln ($2\pi f$) = lnτ_0^{-1} + $\Delta E/(k_B T)$. The energy barrier $\Delta E/k_B$ was 81 K and pre-exponential factor τ_0 was 3.3(4) × 10^{-11} s.

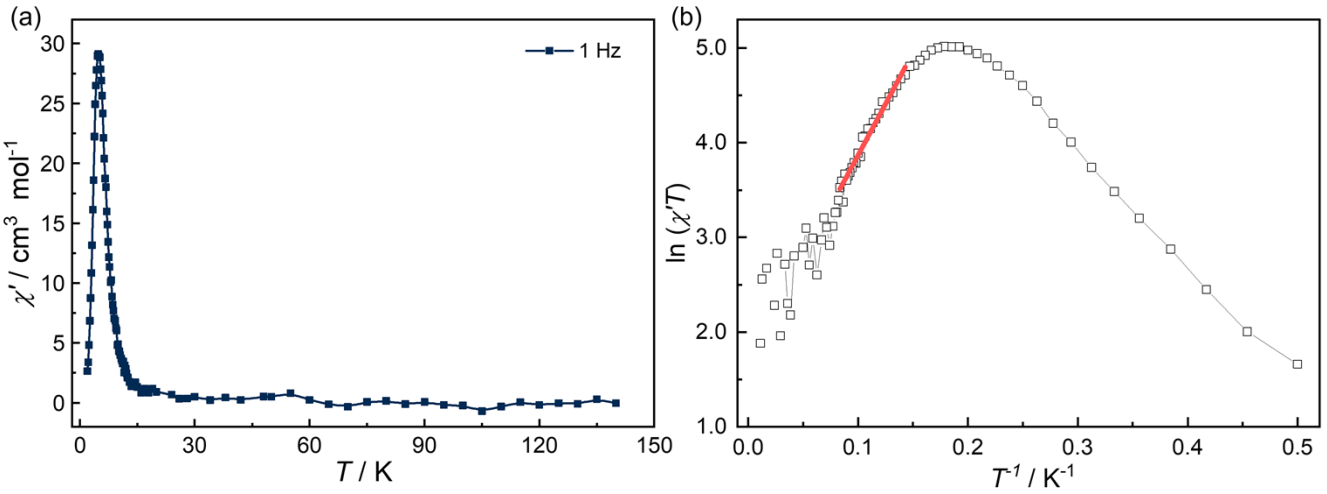

Fig. S15. (a) Temperature dependence of the in-phase of ac magnetic susceptibility of **1** after 946-nm irradiation under zero DC field at 1 Hz. (b) Plot of ln($\chi'T$) versus T^{-1} for **1** after 946-nm irradiation. The red line represented the fitting by applying equation $\chi'T = C_{\text{eff}} \exp(\Delta\zeta/k_{\text{B}}T)$.

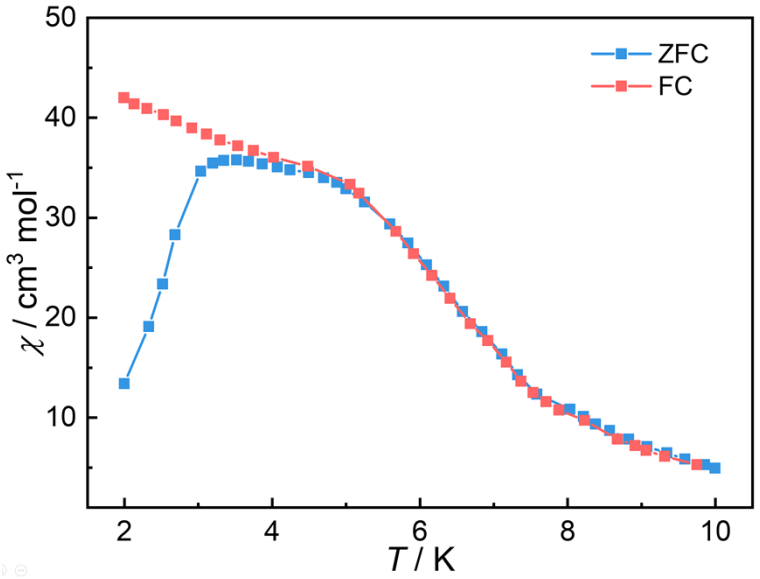

Fig. S16. Zero-field-cooling and field-cooling susceptibility measurement for **1** under 50 Oe DC field after 946-nm light irradiation.

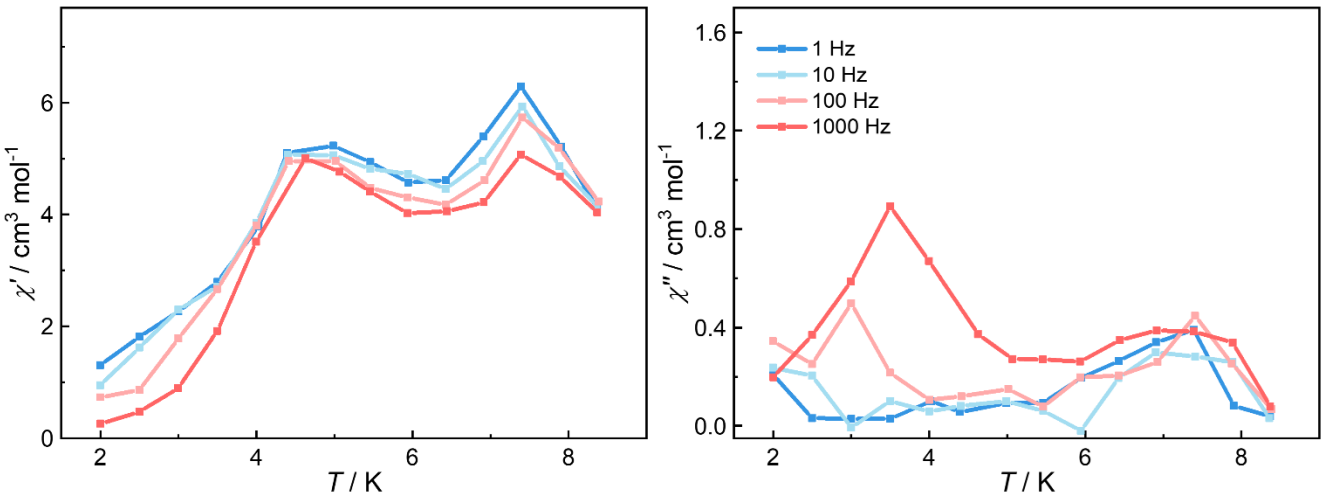

Fig. S17. Temperature dependence of in-phase (χ') and out-of-phase (χ'') signals for **2** after irradiation under zero DC field and 3.5 Oe AC field.

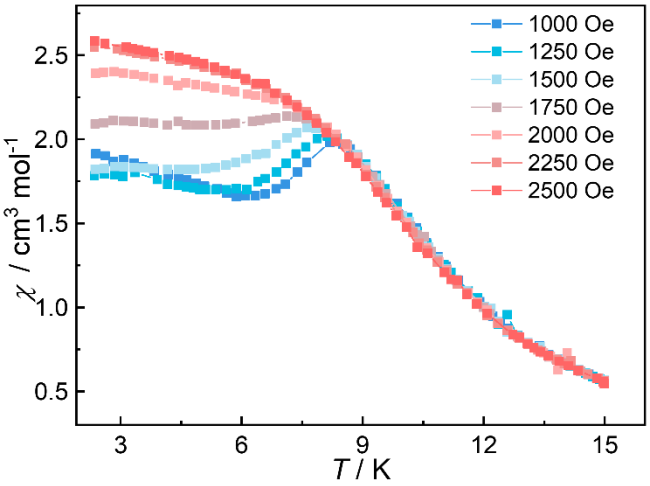

Fig. S18. Susceptibility measurements of compound **2** under different dc fields after light irradiation.

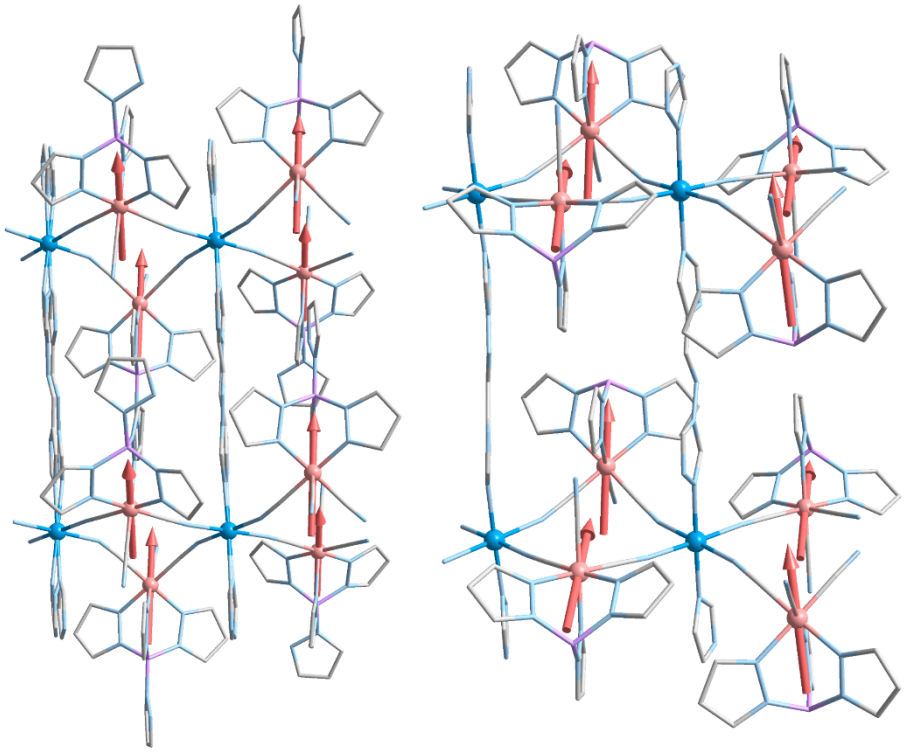

Fig. S19. View of twisted iron cores present in **1** (left) and **2** (right) along the pseudo-*C3* axes (along the B···Fe vectors).

Reference

[S1] D. P. Dong, T. Liu, S. Kanegawa, S. Kang, O. Sato, C. He and C. Y. Duan, Photoswitchable dynamic magnetic relaxation in a well-isolated {Fe_2Co} double-zigzag chain, *Angew. Chem. Int. Ed.*, 2012, **51**, 5119-5123.

[S2] T. Liu, Y. J. Zhang, S. Kanegawa and O. Sato, Photoinduced Metal-to-Metal Charge Transfer toward Single-Chain Magnet, *J. Am. Chem. Soc.*, 2010, **132**, 8250-8251.

[S3] N. Hoshino, F. Iijima, G. N. Newton, N. Yoshida, T. Shiga, H. Nojiri, A. Nakao, R. Kumai, Y. Murakami and H. Oshio, Three-way switching in a cyanide-bridged [CoFe] chain, *Nat. Chem.*, 2012, **4**, 921-926.

[S4] M. Nihei, Y. Okamoto, Y. Sekine, N. Hoshino, T. Shiga, I. P. Liu and H. Oshio, A light-induced phase exhibiting slow magnetic relaxation in a cyanide-bridged [Fe_4Co_2] complex, *Angew. Chem. Int. Ed.*, 2012, **51**, 6361-6364.

[S5] W. Jiang, C. Jiao, Y. Meng, L. Zhao, Q. Liu and T. Liu, Switching single chain magnet behavior via photoinduced bidirectional metal-to-metal charge transfer, *Chem. Sci.*, 2018, **9**, 617-622.

[S6] J. Li, S. Wu, S. Su, S. Kanegawa and O. Sato, Manipulating Slow Magnetic Relaxation by Light in a Charge Transfer {Fe_2Co} Complex, *Chem. Eur. J.,* 2020, **26**, 3259-3263.

[S7] N.-T. Yao, L. Zhao, C. Yi, Q. Liu, Y.-M. Li, Y.-S. Meng, H. Oshio and T. Liu, Manipulating Selective Metal-to-Metal Electron Transfer to Achieve Multi-Phase Transitions in an Asymmetric Fe_2Co-Assembled Mixed-Valence Chain, *Angew. Chem. Int. Ed.*, 2022, DOI: 10.1002/anie.202115367.